LC–PHSM–2003–071
August 2003

Study of Sleptons – Supersymmetry Scenario SPS 1

Hans-Ulrich Martyn

I. Physikalisches Institut, RWTH Aachen, Germany

The properties of the light charged sleptons $\tilde{e}_R$, $\tilde{\mu}_R$ and $\tilde{\tau}_1$ are studied within the mSUGRA scenario SPS 1. The analysis is based on a complete simulation of signal and background reactions assuming experimental conditions of the TESLA e^+e^- Linear Collider.

1 Introduction

Particle spectrum mSUGRA SPS 1 scenario [1] (parameters $m_0 = 100$ GeV, $m_{1/2} = 250$ GeV, $A_0 = -100$ GeV, $\tan\beta = 10$, $\operatorname{sign}\mu +$) shown in fig. 1. Cascade decays of $\tilde{\chi}^0_2$, $\tilde{\chi}^\pm_1$ lead to abundant τ final states.

Event generation PYTHIA 6.2 [2] including QED radiation, beamstrahlung à la CIRCE [3], beam polarisations $\mathcal{P}_{e^\pm}$, τ decays and polarisation treated by TAUOLA [4]

Operating conditions $\sqrt{s} = 400$ GeV, beam polarisations $\mathcal{P}_{e^-} = +0.80$, $\mathcal{P}_{e^+} = -0.60$, integrated luminosity $\mathcal{L} = 200\ \mathrm{fb}^{-1}$

Detector à la TDR Simulation based on SIMDET 4.02 [5], acceptance $\theta > 125$ mrad, e, γ veto $\theta > 4.6$ mrad

Slepton production

$$e^+_L e^-_R \to \tilde{\mu}_R \tilde{\mu}_R \qquad (120\,\mathrm{fb}) \tag{1}$$
$$e^+_L e^-_R \to \tilde{e}_R \tilde{e}_R \qquad (550\,\mathrm{fb}) \tag{2}$$
$$e^+_L e^-_R \to \tilde{\tau}_1 \tilde{\tau}_1 \qquad (140\,\mathrm{fb}) \tag{3}$$

Background production SUSY bkg $e^+_L e^-_R \to \tilde{e}_R \tilde{e}_L\,(75\,\mathrm{fb}),\ \tilde{\chi}^0_2 \tilde{\chi}^0_1\,(20\,\mathrm{fb}),\ \tilde{\chi}^+_1 \tilde{\chi}^+_1\,(5\,\mathrm{fb})$
SM bkg $e^+_L e^-_R \to W^+ W^-\,(1000\,\mathrm{fb})$ $[\ell^+\ell^-(\gamma),\ e^+e^-\ell^+\ell^-]$
$\gamma\gamma$ bkg negligible $\sigma(e^+e^-\tau^+\tau^-) = 4.5 \cdot 10^5$ fb, acceptance $<$ few10^{-6}

Slepton decays

$$\tilde{\ell}^- \quad \to \quad \ell^- \, \tilde{\chi}^0_1 \tag{4}$$

Flat lepton energy spectrum with endpoints $E_{+/-}$ related to slepton and neutralino masses

$$E_{+/-} = \frac{\sqrt{s}}{4}\left(1 - \frac{m^2_{\tilde{\chi}}}{m^2_{\tilde{\ell}}}\right)(1 \pm \beta) \tag{5}$$

$$m_{\tilde{l}} = \frac{\sqrt{s}}{E_- + E_+}\sqrt{E_- E_+} \tag{6}$$

$$m_{\tilde{\chi}} = m_{\tilde{l}}\sqrt{1 - \frac{E_- + E_+}{\sqrt{s}/2}} \tag{7}$$

$\ell^+\ell^-$ momentum correlations
$m_{\tilde{\chi}^0}$ known: energy-momentum conservation constrains
construction of kinematically allowed minimum mass $m_{\min}(\tilde{\ell})$
sharp peak around true mass $m_{\tilde{\ell}}$ [6]

$m_{\tilde{\chi}^0}$ and $m_{\tilde{\ell}}$ known: reconstruct $\tilde{\ell}$ direction θ
two-fold ambiguity, false solution flat in $\cos\theta$

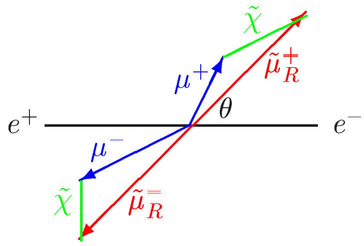

2 Properties of smuons

Selection criteria $e^+_L e^-_R \to \tilde{\mu}_R \tilde{\mu}_R$ at $\sqrt{s} = 400$ GeV

nr	cut	min	max	eff
0.	n_ch, n_gamma in accept.	2	0	0.815
	n_charge in acceptance	2	2	0.989
	n_gamma in acceptance	5.0	0	0.851
	n_veto in acceptance	5.0	0	0.960
1.	Q*cos_theta_l	-0.900	0.750	0.693
2.	delta phi_(l+,l-) (deg)		160.0	0.555
4.	p_T event (GeV)	10.0		0.553
5.	p_miss cos_theta_(l+l-)		0.900	0.537
7.	lepton energy (GeV)	2.5	150.0	0.537
10.	m_recoil + 0.4*m_ll (GeV)	240.0		0.537

efficiency 0.5365

lepton energy E_min 16.52 E_max 93.30

Mass determination Spectra of the muon energy E_μ and minimum mass $m_{\min}(\tilde{\mu}_R)$ are shown in fig. 2. The endpoint energies, $E_- = 16.570 \pm 0.040$ GeV and $E_+ = 93.30 \pm 0.22$ GeV, give strongly correlated $\tilde{\mu}_R$ and $\tilde{\chi}_1^0$ masses. The reconstructed masses from both methods agree well with the input values.

method	$m_{\tilde{\mu}_R}$ [GeV]	$m_{\tilde{\chi}_1^0}$ [GeV]
E_μ **spectrum**	$\mathbf{143.15 \pm 0.17}$	$\mathbf{96.10 \pm 0.21}$
$m_{\min}(\tilde{\mu}_R)$ **spectrum**	$\mathbf{142.98 \pm 0.03}$	**fixed**
SPS 1 input	**143.0**	**96.0**

Spin $J = 0$ of $\tilde{\mu}_R$ The polar angle distribution of $\tilde{\mu}_R\tilde{\mu}_R$ production is presented in fig. 3. After background subtraction on finds the typical cross section dependence

$$\frac{\mathrm{d}\sigma}{\mathrm{d}\cos\theta} \quad \propto \quad \sin^2\theta$$

as expected for a scalar particle.

3 Properties of selectrons

Selection criteria $e_L^+ e_R^- \to \tilde{e}_R \tilde{e}_R$ at $\sqrt{s} = 400$ GeV

```
nr  cut                                 min       max      eff
------------------------------------------------------------
 0. n_ch, n_gamma in accept.              2         0     0.742
    n_charge in acceptance                2         2     0.984
    n_gamma  in acceptance              5.0         0     0.780
    n_veto   in acceptance              5.0         0     0.960
 1. Q*cos_theta_l                    -0.900     0.750     0.586
 2. delta phi_(l+,l-) (deg)                     160.0     0.484
 4. p_T event (GeV)                    10.0               0.484
 5. p_miss cos_theta_(l+l-)                     0.900     0.468
 7. lepton energy (GeV)                 2.5     150.0     0.468
10. m_recoil + 0.4*m_ll (GeV)         240.0               0.468

 efficiency     0.4675

 lepton energy  E_min 16.52       E_max 93.30
```

Mass determination Spectra of the electron energy E_e and minimum mass $m_{\min}(\tilde{e}_R)$ are shown in fig. 4. The endpoint energies, $E_- = 16.528 \pm 0.020$ GeV and $E_+ = 93.34 \pm 0.11$ GeV, give strongly correlated $\tilde{e}_R$ and $\tilde{\chi}_1^0$ masses. The reconstructed masses from both methods are in agreement with the input values.

method	$m_{\tilde{e}_R}$ [GeV]	$m_{\tilde{\chi}_1^0}$ [GeV]
E_e **spectrum**	$\mathbf{142.99 \pm 0.08}$	$\mathbf{96.05 \pm 0.10}$
$m_{\min}(\tilde{e}_R)$ **spectrum**	$\mathbf{142.97 \pm 0.02}$	**fixed**
SPS 1 input	**143.0**	**96.0**

Angular distribution of $\tilde{e}_R$ The polar angle distribution of $\tilde{e}_R\tilde{e}_R$ production is presented in fig. 5. After background subtraction on finds the typical behaviour of t-channel neutralino exchange, given by the approximate matrix element

$$\mathcal{M} \;\sim\; \beta \sin\theta \left[1 - \frac{4\,Y_{\tilde{B}}^2}{1 - 2\,\beta\,\cos\theta + \beta^2 + 4\,M_1^2/s}\right] .$$

The differential cross section can be used to determine the Yukawa coupling $Y_{\tilde{B}} = \hat{g}'_{\tilde{B}\tilde{e}e}/g'_{\gamma ee}$ and the gaugino mass parameter M_1 at the percent level.

Chiral quantum numbers A unique determination of the selectron L/R quantum numbers is offered by the reaction $e^+e^- \to \tilde{e}_R\tilde{e}_L$, which proceed via pure t-channel $\tilde{\chi}^0$ exchange. The 'chiral flow' at the $e\tilde{\chi}^0\tilde{e}$ vertex associates the incoming electron/positron with its superpartner: $e^-_L \to \tilde{e}^-_L$, $e^-_R \to \tilde{e}^-_R$ and $e^+_L \to \tilde{e}^+_R$, $e^+_R \to \tilde{e}^+_L$. Measuring the energy spectra of the decay e^- and e^+ separately allows for a clear distinction between $\tilde{e}_R$ and $\tilde{e}_L$. Moreover, by choosing appropriate beam polarisations, *e.g.* 'odd' combinations $e^+_R e^-_R \to \tilde{e}^+_L\tilde{e}^-_R$ or $e^+_L e^-_L \to \tilde{e}^+_R\tilde{e}^-_L$, one suppresses the s-channel γ, Z amplitudes of $\tilde{e}_R\tilde{e}_R$ and other background and enhances the $\tilde{e}_R\tilde{e}_L$ production considerably, as illustrated in fig. 6 and fig. 7. A measurement of the $\tilde{e}_L$ mass of $m_{\tilde{e}_L} = 202.1 \pm 0.5$ GeV appears feasible. Similar studies are reported in [7].

4 Properties of staus

Parameters $L - R$ mixing in third generation, access to $\tan\beta$ and A_τ [8, 9]

$$\begin{pmatrix} \tilde{\tau}_1 \\ \tilde{\tau}_2 \end{pmatrix} = \begin{pmatrix} \cos\theta_{\tilde{\tau}} & \sin\theta_{\tilde{\tau}} \\ -\sin\theta_{\tilde{\tau}} & \cos\theta_{\tilde{\tau}} \end{pmatrix} \begin{pmatrix} \tilde{\tau}_L \\ \tilde{\tau}_R \end{pmatrix} \tag{8}$$

$$\tan 2\,\theta_{\tilde{\tau}} = \frac{-2\,m_\tau\,(A_\tau - \mu\tan\beta)}{m^2_{\tilde{\tau}_R} - m^2_{\tilde{\tau}_L}} \tag{9}$$

τ polarisation $\mathcal{P}_\tau$ in decay $\tilde{\tau}_1 \to \tau\tilde{\chi}^0_1$ $\qquad \mathcal{P}_\tau = \mathcal{P}_\tau(\theta_{\tilde{\tau}}, \tan\beta, \tilde{\chi}^0_1 \text{ mixing})$

Selection criteria $e^+_L e^-_R \to \tilde{\tau}^+_1\tilde{\tau}^-_1$ at $\sqrt{s} = 400$ GeV

nr	cut	min	max	eff
0.	n_charge, n_veto	2 6	1	0.931
1.	n_jets	2	4	0.834
2.	n_taus	2	4	0.829
3.	n_leptons	0	2	0.780
4.	E_jet (GeV)	2.5	100.0	0.739
5.	Q*cos_theta_jet	-0.950	0.750	0.597
8.	mass tau_jet (GeV)		2.000	0.547
11.	delta phi_(l,di-jet) (deg)		160.0	0.426
12.	cos theta_P_miss		0.95	0.424
13.	p_T (GeV)	10.0	200.0	0.400

efficiency SUSY 0.3999

```
tau decay statistics
--------------------
              e      mu      pi     rho     3_pi      sum
e             0     510     529    1097     1125     3261
mu            0       0     470    1040     1121     2631
pi            0       0     200     783      819     1802
rho           0       0       0     821     1786     2607
3_pi          0       0       0       0      895      895
sum           0     510    1199    3741     5746    11196

 lepton energy       E_min 12.19       E_max 83.81
```

Leptonic τ decays not useful and discarded due to large WW background
Analysed decay modes & branching ratios

$$\mathcal{B}(\tau \to \pi\nu_\tau) = 0.111,\ \mathcal{B}(\tau \to \rho\nu_\tau) = 0.254,\ \mathcal{B}(\tau \to 3\pi\nu_\tau) = 0.194$$

$m_{\tilde{\tau}_1}$ from τ decays $\quad \tau \to \rho\ \nu_\tau \to \pi^\pm\pi^0\ \nu_\tau$ and $\tau \to 3\pi\ \nu_\tau \to \pi^\pm\pi^\pm\pi^\mp\ \nu_\tau + \pi^\pm\pi^0\pi^0\ \nu_\tau$
E_ρ, $E_{3\pi}$ sensitive to $m_{\tilde{\tau}_1}$, almost independent of $\mathcal{P}_\tau$

Analysis of E_ρ and $E_{3\pi}$ spectra, shown in fig. 8, assuming $m_{\tilde{\chi}_1^0}$ known

mode	$m_{\tilde{\tau}_1}$ [GeV]
E_ρ	133.3 ± 0.75
$E_{3\pi}$	133.2 ± 0.30
mean	133.2 ± 0.30
SPS 1 input	133.2

$\theta_{\tilde{\tau}}$ from cross section $\quad$ A cross section measurement of $\sigma_{\tilde{\tau}_1\tilde{\tau}_1} = 137.8 \pm 2.2_{\rm stat} \pm 1.4_{\rm sys}$ fb (incl. ISR & BS) provides a $\tilde{\tau}$ mixing angle of $\cos 2\,\theta_{\tilde{\tau}} = -0.84 \pm 0.04$, see fig. 10

τ polarisation $\mathcal{P}_\tau$ $\quad E_\pi$ from $\tau \to \pi\ \nu_\tau$ and $z_\pi = E_\pi/E_\rho$ from $\tau \to \rho\nu_\tau \to \pi\pi^0\nu_\tau$
E_π, z_π sensitive to $\mathcal{P}_\tau$, almost independent of $m_{\tilde{\tau}_1}$

τ is self-analysing system – spin correlations

$\tau_R^- \to \pi^-\nu \quad \mathcal{P}_\tau = +1 \quad \pi^-$ emitted in forward direction $\quad E_\pi \nearrow$
$\tau_L^- \to \pi^-\nu \quad \mathcal{P}_\tau = -1 \quad \pi^-$ emitted in backward direction $\quad E_\pi \searrow$

$\tau_R^- \to \rho_L^-\nu \quad \mathcal{P}_\tau = +1 \quad {\rm d}\sigma/{\rm d}z_\pi \propto (2z_\pi - 1)^2$ $\quad$ asymmetric sharing $z_\pi \to 0\,/\,1$
$\tau_L^- \to \rho_T^-\nu \quad \mathcal{P}_\tau = -1 \quad {\rm d}\sigma/{\rm d}z_\pi \propto 2z_\pi(1 - z_\pi)$ $\quad$ equal sharing $z_\pi \to 0.5$

Analysis of E_π and z_π spectra, shown in fig. 9, $m_{\tilde{\chi}_1^0}$ assumed to be known

mode	$\mathcal{P}_\tau$
E_π	0.98 ± 0.045
$z_\pi = E_\pi/E_\rho$	1.02 ± 0.038
mean	1.00 ± 0.035
SPS 1 input	0.981

A polarisation measurement of $\mathcal{P}_\tau = 1.00 \pm 0.035$ is not sensitive enough to determine $\tan\beta$ in SPS 1, where one has $\delta\mathcal{P}_\tau/\delta\tan\beta = 0.3\%$

5 Summary

Simulations of slepton production $e^+e^- \to \tilde{e}_R\tilde{e}_R,\ \tilde{\mu}_R\tilde{\mu}_R,\ \tilde{\tau}_1\tilde{\tau}_1$ in the SPS 1 mSUGRA scenario under realistic experimental conditions assuming $\sqrt{s} = 400$ GeV, $\mathcal{L} = 200$ fb^{-1} and beam polarisations $\mathcal{P}_{e^-} = +0.8$, $\mathcal{P}_{e^+} = -0.6$ are presented. The slepton and neutralino $\tilde{\chi}^0_1$ masses as well as the polarisation $\mathcal{P}_{\tilde{\tau}_1\to\tau\tilde{\chi}^0_1}$ and mixing parameter $\theta_{\tilde{\tau}}$ of the third generation can be accurately determined with moderate integrated luminosity. Improvements on $m_{\tilde{e}_R}$ and $m_{\tilde{\mu}_R}$ are possible if $\delta m_{\tilde{\chi}^0_1}$ can be reduced, *e.g.* by studying neutralino production and decays. Other estimates on SPS 1 sparticle masses can be found in [7] and [10] (not based on detailed simulations).

$\tilde{e}_R$	$m_{\tilde{e}_R} = 142.99 \pm 0.08$ GeV	$m_{\tilde{\chi}^0_1} = 96.05 \pm 0.10$ GeV
$\tilde{\mu}_R$	$m_{\tilde{\mu}_R} = 143.15 \pm 0.17$ GeV	$m_{\tilde{\chi}^0_1} = 96.10 \pm 0.21$ GeV
$\tilde{\tau}_1$	$m_{\tilde{\tau}_1} = 133.2 \pm 0.30$ GeV	—
	$\cos 2\,\theta_{\tilde{\tau}} = -0.84 \pm 0.04$	$\mathcal{P}_\tau = 1.00 \pm 0.035$

Acknowledgement I want to thank G. Moortgat-Pick for the stimulating discussions on the stau sector and for providing the plot of fig. 10.

References

[1] N. Ghodbane, H.-U. Martyn, hep-ph/0201233; B.C. Allanach et al., Eur. Phys. J. C 25 (2002) 113.

[2] PYTHIA, T. Sjöstrand et al., Comput. Phys. Commun. 135 (2001) 238.

[3] CIRCE, T. Ohl, Comput. Phys. Commun. 101 (1997) 269.

[4] TAUOLA, S. Jadach et al., Comput. Phys. Commun. 76 (1993) 361.

[5] SIMDET, M. Pohl, J. Schreiber, DESY-02-061, hep-ex/0206009.

[6] J. Feng, D. Finell, Phys. Rev. D 49 (1994) 2369.

[7] M. Dima et al., Phys. Rev. D 65 (2002) 71701.

[8] M.M. Nojiri, Phys. Rev. D 51 (1995) 6281; M.M. Nojiri, K. Fujii, T. Tsukamoto, Phys. Rev. D 54 (1996) 6756.

[9] E. Boos et al., hep-ph/0303110, DESY 03-030, accepted by EPJC.

[10] P. Grannis, talk at LCWS 02, Jeju Island, Korea, 2002, hep-ex/0211002.

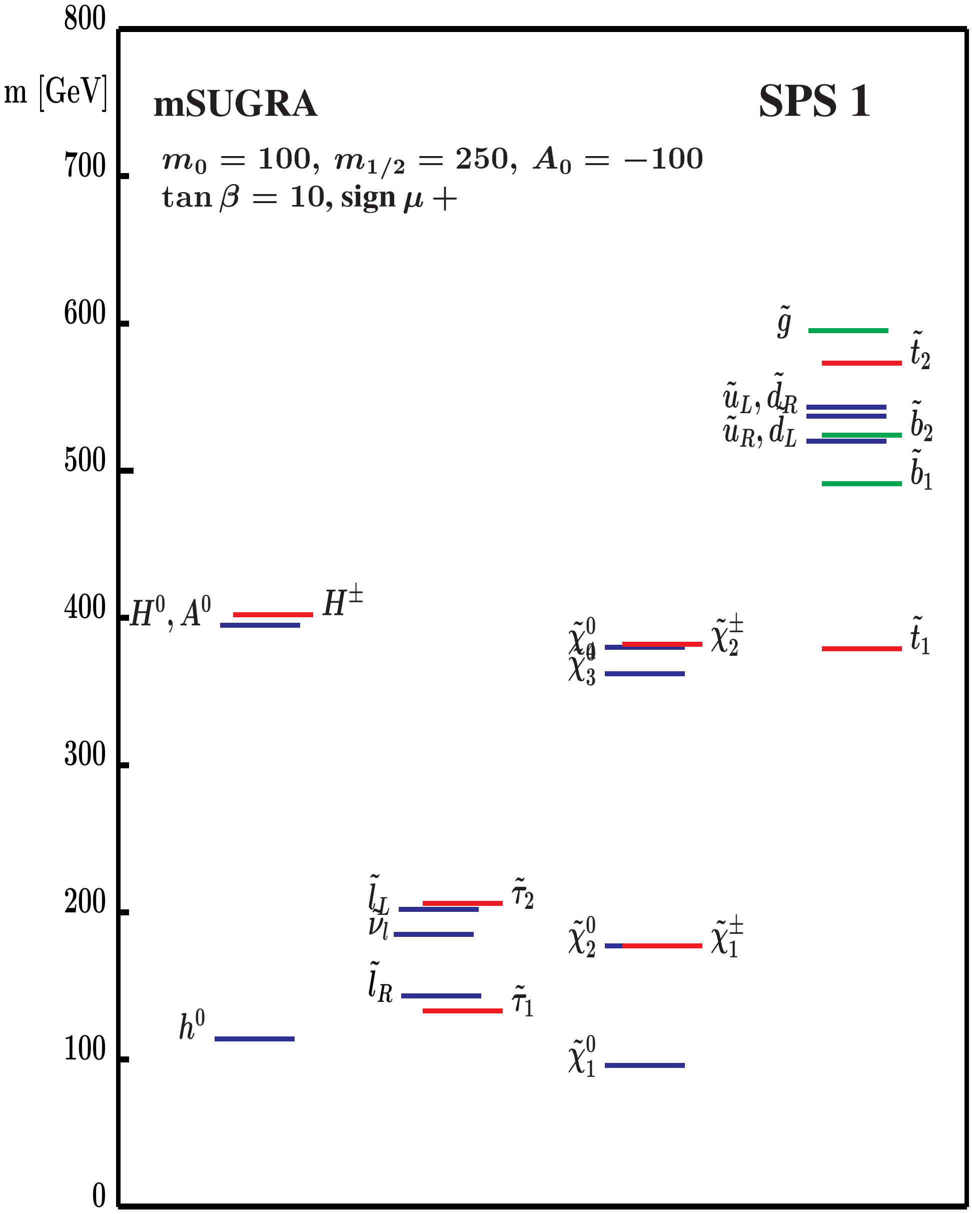

Figure 1: Particle spectrum of mSUGRA benchmark scenario SPS 1

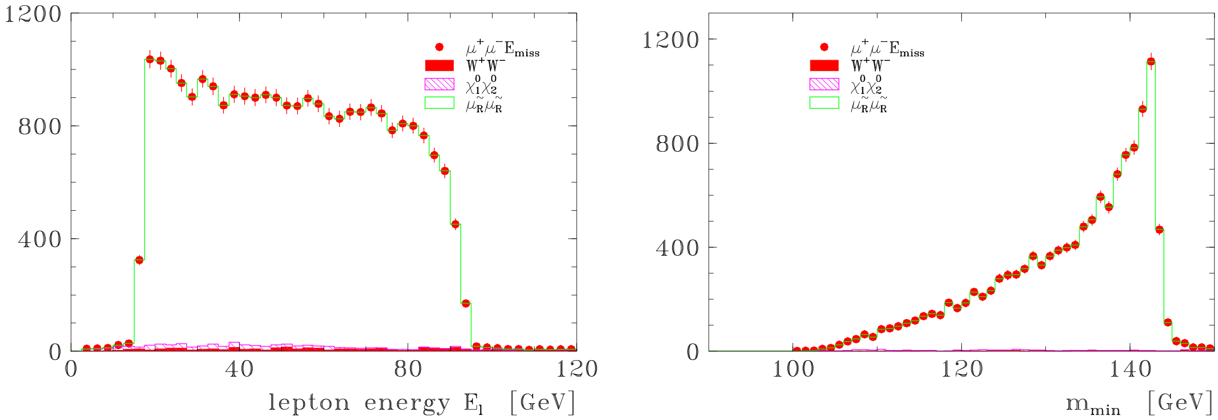

Figure 2: Energy spectrum E_μ of muons (left) and minimum mass $m_{\min}(\tilde{\mu}_R)$ (right) from the reaction $e^+_L e^-_R \to \tilde{\mu}^+_R \tilde{\mu}^-_R \to \mu^+ \tilde{\chi}^0_1\ \mu^- \tilde{\chi}^0_1$; mSUGRA model SPS 1 at $\sqrt{s} = 400$ GeV and $\mathcal{L} = 200$ fb^{-1}

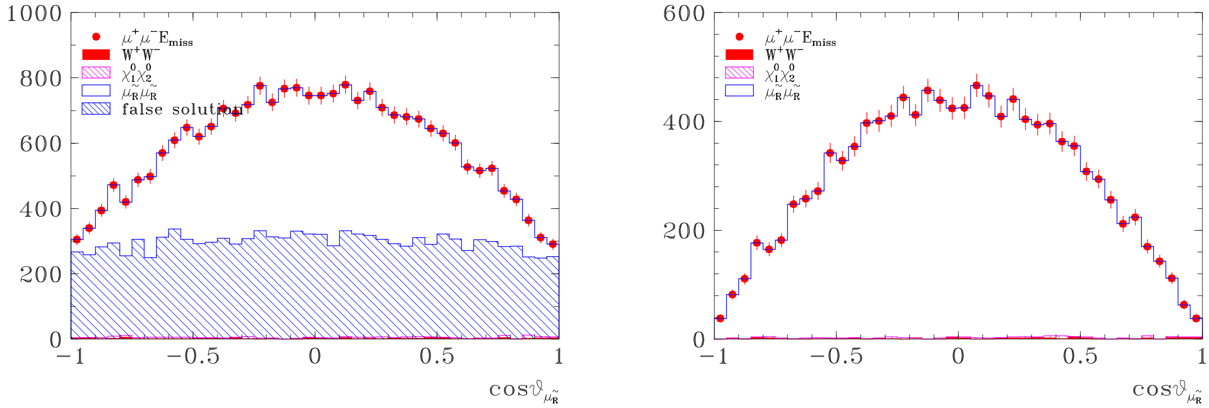

Figure 3: Polar angle distribution of $\tilde{\mu}_R$ with (left) and without (right) contribution of false solution in the reaction $e^+_L e^-_R \to \tilde{\mu}^+_R \tilde{\mu}^-_R \to \mu^+ \tilde{\chi}^0_1\ \mu^- \tilde{\chi}^0_1$; mSUGRA model SPS 1 at $\sqrt{s} =$ 400 GeV and $\mathcal{L} = 200$ fb^{-1}

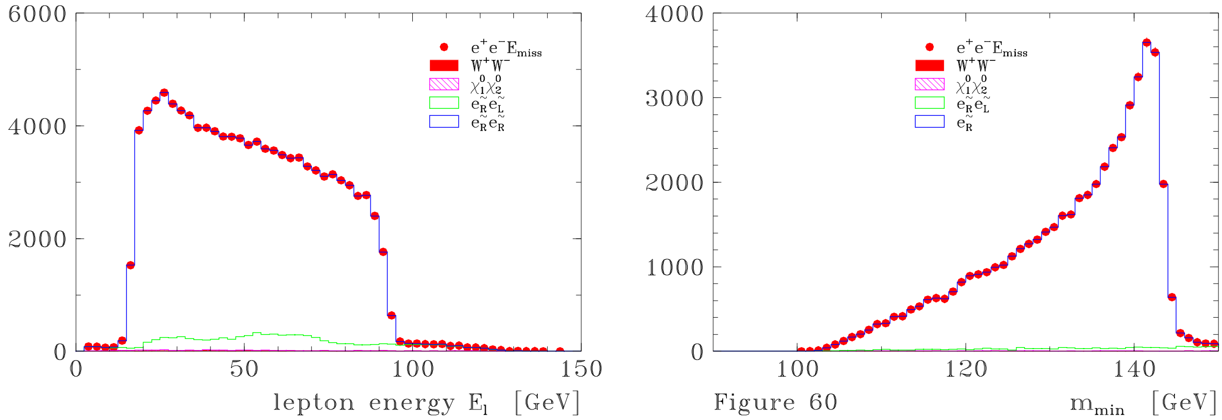

Figure 4: Energy spectrum E_e of electrons (left) and minimum mass $m_{\min}(\tilde{e}_R)$ (right) from the reaction $e^+_L e^-_R \to \tilde{e}^+_R \tilde{e}^-_R \to e^+ \tilde{\chi}^0_1 \, e^- \tilde{\chi}^0_1$; mSUGRA model SPS 1 at $\sqrt{s} = 400$ GeV and $\mathcal{L} = 200$ fb^{-1}

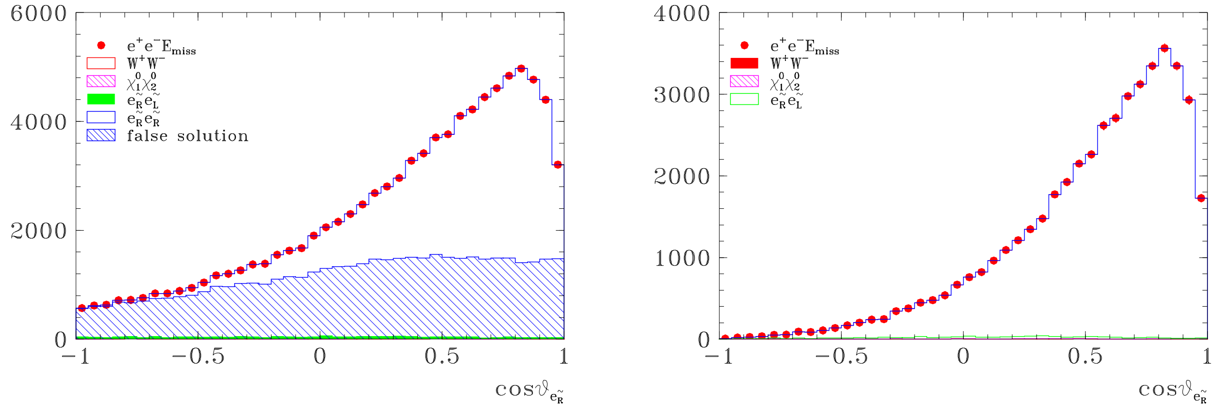

Figure 5: Polar angle distribution of $\tilde{e}_R$ with (left) and without (right) contribution of false solution in the reaction $e^+_L e^-_R \to \tilde{e}^+_R \tilde{e}^-_R \to e^+ \tilde{\chi}^0_1 \, e^- \tilde{\chi}^0_1$; mSUGRA model SPS 1 at $\sqrt{s} =$ 400 GeV and $\mathcal{L} = 200$ fb^{-1}

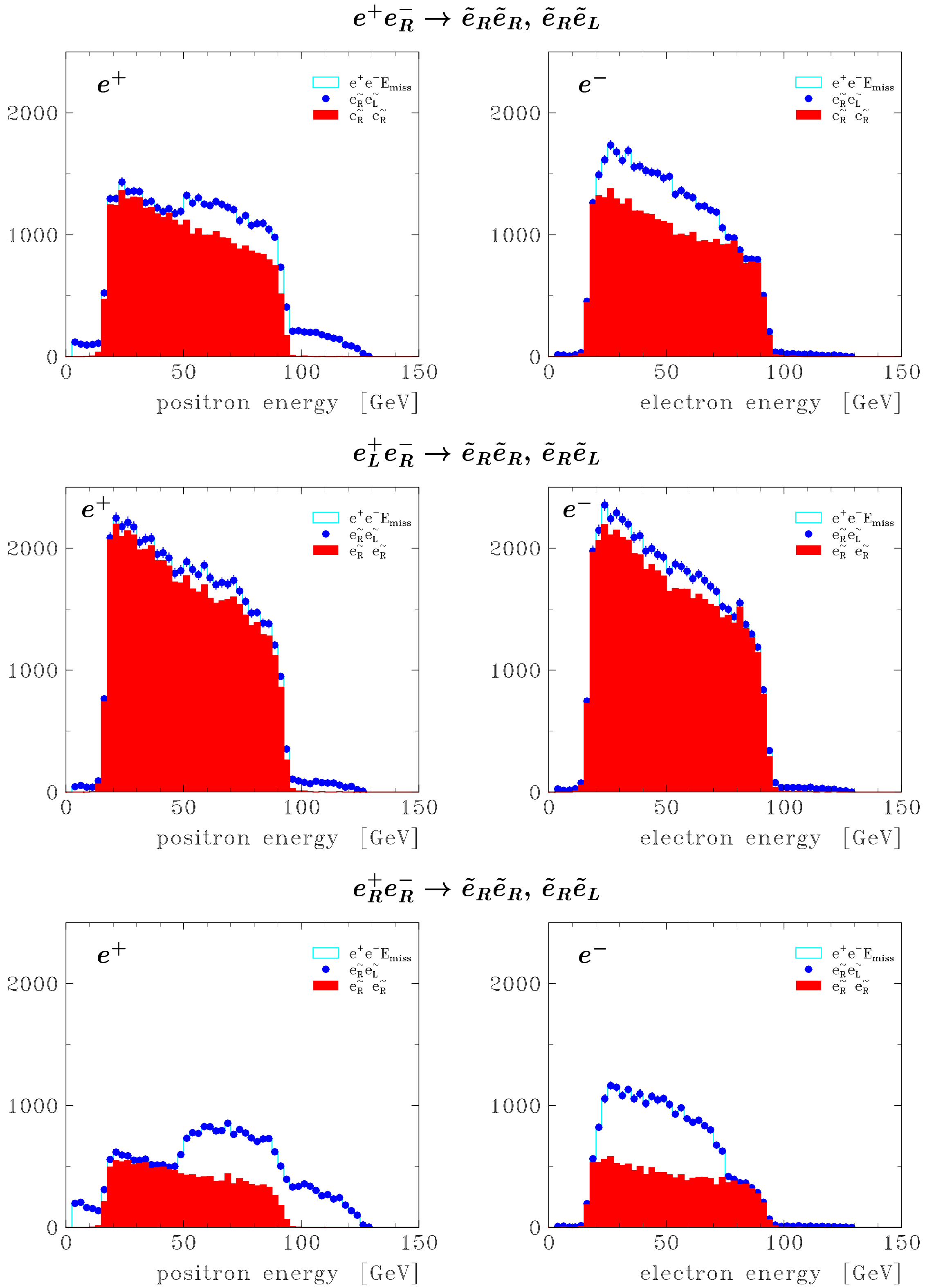

Figure 6: $e^{\pm}$ energy spectra from $e^+e^- \to \tilde{e}_R\tilde{e}_R + \tilde{e}_R\tilde{e}_L$ production with polarisations $\mathcal{P}_{e^-} = +0.8$, $\mathcal{P}_{e^+}$ variable for SPS 1 scenario assuming $\sqrt{s} = 400\,\mathrm{GeV}$ and $\mathcal{L} = 200\,\mathrm{fb}^{-1}$

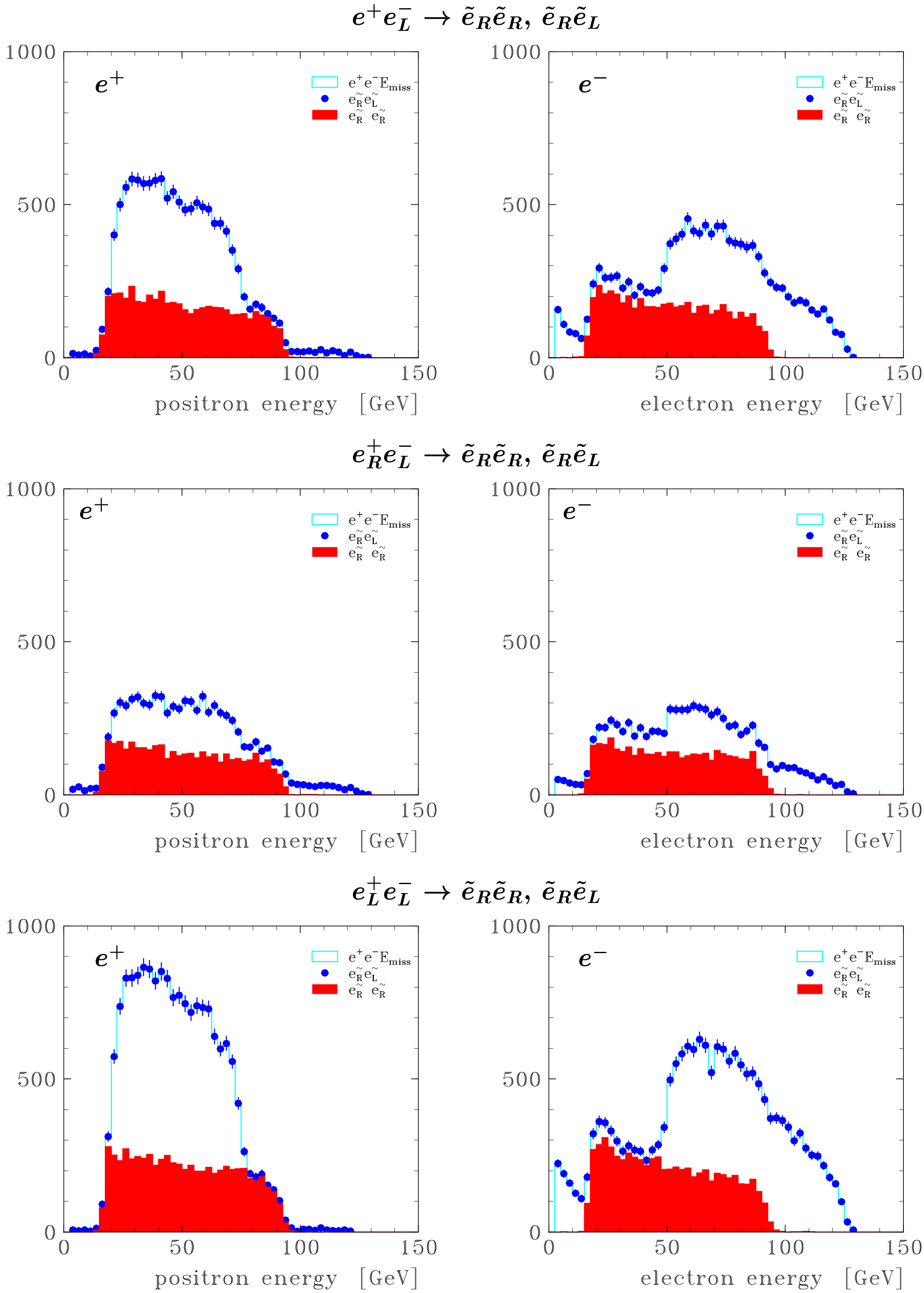

Figure 7: $e^{\pm}$ energy spectra from $e^+e^- \to \tilde{e}_R\tilde{e}_R + \tilde{e}_R\tilde{e}_L$ production with polarisations $\mathcal{P}_{e^-} = -0.8$, $\mathcal{P}_{e^+}$ variable for SPS 1 scenario assuming $\sqrt{s} = 400\,\mathrm{GeV}$ and $\mathcal{L} = 200\,\mathrm{fb}^{-1}$

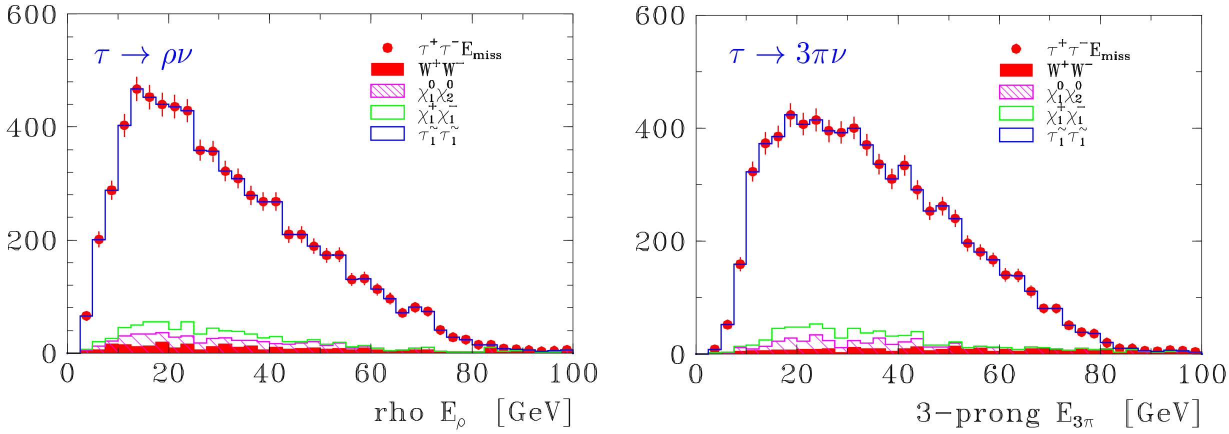

Figure 8: Hadron energy spectra E_ρ of $\tau \to \rho\nu_\tau$ and $E_{3\pi}$ of $\tau \to 3\pi\nu_\tau$ decays from the reaction $e_L^+ e_R^- \to \tilde{\tau}_1^+ \tilde{\tau}_1^1 \to \tau^+ \tilde{\chi}_1^0\ \tau^- \tilde{\chi}_1^0$ in SPS 1 scenario assuming $\sqrt{s} = 400\,\mathrm{GeV}$ and $\mathcal{L} = 200\,\mathrm{fb}^{-1}$

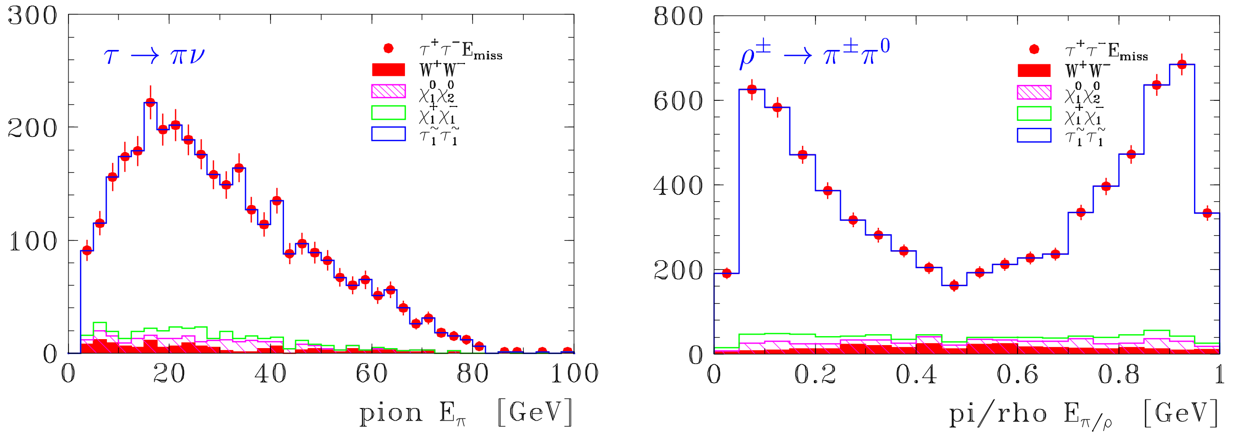

Figure 9: Pion energy spectrum E_π of $\tau \to \pi\nu_\tau$ and ratio $z_\pi = E_\pi/E_\rho$ of $\tau \to \rho\nu_\tau$ decays from the reaction $e_L^+ e_R^- \to \tilde{\tau}_1^+ \tilde{\tau}_1^1 \to \tau^+ \tilde{\chi}_1^0\ \tau^- \tilde{\chi}_1^0$ in SPS 1 scenario assuming $\sqrt{s} = 400\,\mathrm{GeV}$ and $\mathcal{L} = 200\,\mathrm{fb}^{-1}$

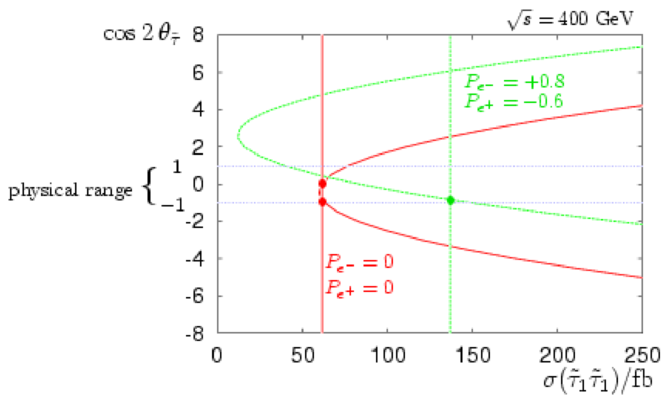

Figure 10: Mixing angle angle $\cos 2\theta_{\tilde{\tau}}$ versus cross section $\sigma_{\tilde{\tau}_1\tilde{\tau}_1}$ at $\sqrt{s} = 400$ GeV for mSUGRA scenario SPS 1